1986

Stress Monitor in High-Pressure Cylinder of Reciprocating Compressor

D. Wang

Y. Zhang

STRESS MONITOR IN HIGH-PRESSURE CYLINDER OF RECIPROCATING COMPRESSOR

Wang Di-sheng, Associate professor, Xi'an Jiaotong University, China

Zhang Yong, Teacher, Xi'an Jiao University, China

ABSTRACT

The economic indexes in fact are affected by the reliability of compressor, which makes it necessary to optimize the construction of compressor parts so as to uniform the stress distribution in them. This paper, as the first parts of the above mentioned work concerns primarily on the computer program and analyzing the distribution of static and dynamic stress in the high pressure cylinder of compressor by means of finite element analysis method of three dimention, and designs a special system which can be used in moniting the dynamic stresses in the cylinder body with the pulsation of the high pressure gas force in the cylinder. The result shows that there exists an optimum construction of cylinder which is connected mainly with the parameters of compressor. This makes it possible to find an optimal structure of cylinder which has a more uniform stress distribution.

I INTRODUCTION

The cylinder is the vital part of a high pressure compressor. Its shapal complexity, further influenced by the fact that it is working under high pressure pulsating gaseous forces, often leads to cylinder failures owing to severe non-uniformity of stress distribution - i.e. stress concentrations. Obviously such failured are very costly, and it is vitally important to strife to improve the reliability of the high pressure cylinder.

Some work on the strength of high pressure cylinders[1][2]has been done in recent years, but such works are chiefly concerning static conditions. This paper, however, presents the results of research on the mathematical model reflecting the afore-mentioned characteristic features of the compressor's high pressure cylin-

der, for which a 3-dimensional finite element method is employed to analyse and evaluate the static and dynamic stresses of the cylinder. Figure 1 shows the flow-chart of such a program which allows the automatic mesh generation of the elements and thus saving up to about 87% of the laborious work of data processing. In order that verification of the analytical results may be obtained, special devices are employed to measure and detect the responses to the dynamic stresses in the high pressure cylinder.

Results show that responses to the dynamic stresses of the high pressure cylinder as predicted by analysis agree satisfactorily close to those frame test. It is thus reasonable to assume both the program and the testing device may be used as a means of calibration of the compressor cylinder. Furthermore, they may be utilized to analyze the effect of other parameters such as suction and exhaust pressure, pressure ratio, revolutionary speed of crank shaft, etc. upon the cylinder's dynamic stresses.

II. DYNAMIC MODEL OF THE CYLINDER

Choosing the critical points under static loads as given by analyses in Ref. 1 and 2 , and taking into account of the cylinder's symmetry, one quarter of the cylinder, i.e. the intersecting portion between the cylinder proper and the exhaust valve is taken as sufficient for the purpose of analysis.

Considering the various forces acting upon the cylinder and the constraining conditions, the following mathematical model for the cylinder is obtained

$$B^T\left(\frac{\partial}{\partial x}\frac{\partial}{\partial y}\frac{\partial}{\partial \beta}\right)[D]B\left(\frac{\partial}{\partial x}\frac{\partial}{\partial y}\frac{\partial}{\partial \beta}\right)\{U\}+\{F\}+\{\rho G(t)\}=\rho\frac{\partial}{\partial t^2}\{U\} \tag{1}$$

$$\{U\}_{\Sigma_1}=0 \tag{2}$$

$$B^T[\cos(n,x),\cos(n,y),\cos(n,\beta)][D]B\left(\frac{\partial}{\partial x}\frac{\partial}{\partial y}\frac{\partial}{\partial \beta}\right)\{U\}_{\Sigma_2}=\{P\} \tag{3}$$

$$\{U(x,y,\beta,t)\}\Big|_{t=0}=\{U_0(x,y,\beta)\} \tag{4}$$

$$\frac{\partial}{\partial t}\{U(x,y,\beta,t)\}_{t=0}=0 \tag{5}$$

where (1) is the differential equation of motion, (2) and (3) the boundary conditions and (4) and (5) the initial conditions.

$$B(\alpha,\beta,\gamma) = \begin{bmatrix} \alpha & o & o \\ o & \beta & o \\ o & o & \gamma \\ \beta & \alpha & o \\ o & \gamma & \beta \\ \gamma & o & \alpha \end{bmatrix}$$

$$D = ds \begin{bmatrix} 1 & \lambda & \lambda & o & o & o \\ \lambda & 1 & \lambda & o & o & o \\ \lambda & \lambda & 1 & o & o & o \\ o & o & o & G & o & o \\ o & o & o & o & G & o \\ o & o & o & o & o & G \end{bmatrix}$$

$$\lambda = \frac{\mu}{1-\mu} \; ; \quad G = \frac{1-2\mu}{2(1-\mu)} \; ; \quad ds = \frac{E(1-\mu)}{(1+\mu)(1-2\mu)};$$

in which μ is Piosson's ratio and E Young's modulus

$$Z_1 = \{(x,y,z,t),\ (x,y,z) \in R_1, \qquad o < t \leq T\}$$

$$Z_2 = \{(x,y,z,t),\ (x,y,z) \in R_2, \qquad o < t \leq T\}$$

R_1 the boundary of cylinder's given displacements, R_2 the boundary of given forces, $R_1 \cup R_2 = 2\Omega$, where Ω being the region surrounded by the cylinder surface.

$\{P\}$ Load vectors on loaded surface

$\{U_o\ (x,y,z)\}$ Initial displacement vector under static load

The appropriate dynamic and static equations are obtained through transformations of the above equations as follows :

Assume that the displacement functions for the inner part of the cylinder, $\{u\ (x,y,z,t)\}$ are compsised from two sets, one being those due to static loads, $\{u_o(x,y,z)\}$ and the other, $\{u_1\ (x,y,z,t)\}$, due to loads, i.e.

$$\{u\ (x,y,z,t)\} = \{u_o(x,y,z)\} + \{u_1\ (x,y,z)\} \qquad (6)$$

Substituting (6) into (1), and by using variational method with appropricate boundary conditions the following are obtained:

Static Equations

$$\begin{cases} D(\phi, u_o) = (F, \phi) + \int_{R_2} \int \phi^T P_o \, ds \\ \{U_o\} \mid R_1 = \{U\} \end{cases} \tag{7}$$

Dynamic Equations

$$\begin{cases} \frac{\partial}{\partial t^2}(\rho u, \phi) + D(u, \phi) = (\rho G(t), \phi) + \int_{R_2} \int \phi^T P_1 \, ds \\ (u, \phi) \mid_{t=o} = \{0\} \\ \frac{\partial}{\partial t}(u, \phi) \mid_{t=o} = \{0\} \end{cases} \tag{8}$$

where

$$D(\phi, \psi) = \iiint_{\Omega} [B(\frac{\partial}{\partial x} \frac{\partial}{\partial y} \frac{\partial}{\partial z}) \psi]^T [D] B(\frac{\partial}{\partial x} \frac{\partial}{\partial y} \frac{\partial}{\partial z}) \phi \, dx \, dy \, dz \tag{9}$$

$$(\phi, \psi) = \iiint_{\Omega} \psi^T \phi \, dx \, dy \, dz \tag{10}$$

Obviously, the variation of the gaseous forces within the cylinder is extremely complicated, nevertheless, we can always expect that these forces are the resultants of a set of stationary non-pulsative pressures and one of pulsating forces of various orders of frequencies. This can be expressed as

$$p = \frac{p_s(1+\varepsilon)}{2} + \sum_{m=1}^{\infty} \frac{z p_s (1-\varepsilon)}{(2m-1)\pi} \sin (2m-1)\omega t \tag{11}$$

where $\varepsilon = \frac{p_d}{p_s}$ is the pressure ratio

In computation, the result is obtained by superposing the stresses due to the pulsating pressures of various orders

III PROGRAMMING

1. Automatic Mesh Generation

The work involved in element meshing chiefly concerns with that of assigning message to the nodes (node numbers, nodal co-ordinates and nodal constraints)and message to the elements (element numbers, physical characteristic of elements, and list relating the global and local codes for the nodal points of the elements).

As shown in Fig.2 we have chosen a 3-dimensional model for the compressor's integral high pressure cylinder, with the parallelepiped of 20 nodal points, which necessitates an excessive amount of labor in data manipulation and input. It is therefore mandatory to first write a subroutine for the error-free and automatic generation of element meshes.

The cylinder body may be looked upon as a region surrounded by its surfaces. As such a region is complex in nature, it is divided into four sub-regions I, II, III and IV of simpler shape and these sub-region are meshed in turn accordingly. Finally assign identical numbers to points on the interfaces of the sub-regions.

For the meshing of the elements of each sub-region as a 3-dimensional problem, it is necessary to provide three mesh-generating lines along three directions, and the numbering of the elements and nodal points is in turn additive along the three lines , which are taken as follows. Take radial direction of the valve chamber as the third generating line, with l,m,n denoting respectively the mesh number on the three lines. The code numbers are generated by first taking m=n=1 and ℓ from 1 to its maximum number l_{max} . For each increment of ℓ , the code number is also increased by 1. The above procedure is applied reiteratively for m = 2, n = 1 (until $m = m_{max}$) and for n = 2 , ... (until $m = m_{max}$) so that finally the total assembly elements have been covered.

The calculation of nodal co-ordinates is carried out in two steps. First, determine all the co-ordinates on the front and rear surfaces of the sub-regions from the input values of co-ordinates of the boundaries of the sub-regions. Second, from the co-ordinates of the front and rear surfaces of the sub-regions, the total assembly of all the points of the entire cylinder can be obtained.

The constraint conditions of all the nodal points are automatically generated at the same time of element meshing. The code numbers of the nodal points on the boundary surfaces are stored in the integer array KK indentifying the nodal constraints. For internal points (i.e. those not on the surfaces of the cylinder as arbitrarily given as - 1 , and the code numbers of two (or three) surfaces are stored in the contraint numbers of the corresponding bi-surfacial or tri-surfacial intersections.

Certain control parameters have to be input to specify the number and dimensions of the meshed elements. Vary these parameters will result in different patterns of meshing, so that comparative study may be carried out simply by varying these parameters.

It should be mentioned that the sub-routine for automatic mesh possesses the ability of detecting accumulative errors during the process of computation.

2. Formation of Stiffness Matrix and Load Vector

Both the stiffness matrix and the load vector are formed by the Gauss integral, which gives the coefficients and automatically arranged to form the respective matrix and vector. In addition, the subroutine LOADR is to used to form the load vector.

3. Static Analysis

The static equations (7) of the discreted system is formed after the stiffness matrix and load vector have been obtained, whose solution in facilitated by the use of LDt method incorporated in the SOLVI sub-routine. Since the equation of the order up to 1000, accuracy unavoidably deteriorates after a certain number of cycles of back substition. In order to overcome this obstacle, over-relaxation with iterative correction procedure is used, the resudual error being stored in double-precision to ensure accuracy.

The nodal stresses are obtained by applying subroutine STRES to the already available nodal displacements.

4. Dynamic Analysis

After discreting the spatial variables, a set of 2nd degree ordinary differential equations with respect to time is obtained.

$$\begin{cases} [C]\dfrac{d^2}{dt^2}\{a\} + [K]\{a\} = \{F(t)\} \\ \{a\}\,|_{t=o} = 0 \\ \{\bar{a}\}\,|_{t=o} = 0 \end{cases} \tag{12}$$

where :

$$[C] = \begin{bmatrix} (\rho\phi_1, \phi_1) & \cdots & (\rho\phi_{3n}, \phi_1) \\ \vdots & & \\ (\rho\phi_1, \phi_{3n}) & \cdots & (\rho\phi_{3n}, \phi_{3n}) \end{bmatrix}$$

$$K = \begin{bmatrix} D(\phi_1, \phi_1) & \cdots & D(\phi_{3n}, \phi_1) \\ \vdots & & \\ D(\phi_1, \phi_{3n}) & \cdots & D(\phi_{3n}, \phi_{3n}) \end{bmatrix}$$

$$\{a\} = [\, a_1 \ \cdots \ a_{3n} \,]^T$$

$$F(t) = \begin{bmatrix} (\rho G(t), \phi_1) + \iint_{R_2} \phi_1^T p_1 ds \\ \vdots \\ (\rho G(t), \phi_{3n}) + \iint_{R_2} \phi_{3n}^T p_1 ds \end{bmatrix}$$

in which n is the number of nodes on outside region R_1.

Simplication is imperative because of the vast number of coupled equations.

Assume :

$$\{a\} = [A_N]\{a_N\} \tag{13}$$

Since [An] are orthogonal modal matrices, the above equations are reduced to.

$$\begin{cases} \{a_N\} + [k_N]\{a_N\} = \{\bar{G}\} \\ \{a_N\}\big|_{t=o} = 0 \\ \{a_N\}\big|_{t=o} = 0 \end{cases} \tag{14}$$

in which :

$$[k_N] = \begin{bmatrix} p_1^2 & & o \\ & \ddots & \\ o & & p_{NS}^2 \end{bmatrix}$$

p_i^2 being the square of eigen-frequencies of various orders of the cylinder and

N_s the order of the required eign-frequencies

$$\{\bar{G}\} = [A_N]^T \{F(t)\} \tag{15}$$

Assuming the frequencies of vibration of the compressor are close to those of the gaseous forces, and considering the nature of variation of cylinder stresses will time, we have the following solutions

$$a_{Nj} = \frac{g_j^{(i)}}{p_j^2 - (2i-1)^2\omega^2}\left[\sin(2i-1)\omega t - \frac{(2i-1)\omega}{p_j}\sin(p_j t)\right] \tag{16}$$

in which :

$g_j^{(i)}$ - j^{th} component in the orthogonal coordinates of the i^{th} forces

ω - angular frequency of crank-shaft.

The manner of variation of the i^{th} force displacement of the j^{th} orthogonal co-ordinate is thus known.

The program enables us to determine the displacement in orthogonal co-ordinates due to the gaseous force of any order at any instant. By (13) these co-ordinates may be transformed to the cylinder's global coordinates and then sub-routine STRES will give the nodal stresses due to the gaseous force of that order at that instant.

It is seen that the stress variation within the cylinder may be simulated and evaluated by computerization.

IV APPLICATION

The cylinder as shown in Fig.1 is subject to static and dynamic analyses as well as actual tests by the above mentioned program and the testing apparatus for this purposes. Described below and the main results obtained.

1. In the static analysis, the stress distribution within the cylinder due to the average gaseous forces from (11) is examined. Fig. 3 and Fig 4 show the stress distribution along the three directions distribution of the plate bore between the valve and cylinder chamber. It is readily seen that the stresses within a cylinder is extremely non-uniform, resulting in high stress concentrations.

The static stresses tend to a maximum on the boundary of the plate bore between the valve and cylinder chamber, indicating this to be a critical region. The above result is in agreement with those by analysis and experiment described in [1], [2].

2. Dynamic Analysis

(1) Effect of gaseous forces

The stress variation due to the gaseous forces of first

4 modes is illustrated in Fig 5 (a),(b) which show that the gaseous stresses within the cylinder not only varies with the gaseous forces but also exhibit some pulsative nature. It is therefore resonable to suppose that the cylinder stresses are superposed from a set of stresses of low frequencies and high amplitudes and another of high frequencies and low amplitudes.

From the findings of fracture mechanics, it is known that under the above conditions of combined various amplitudes and frequencies the crack growth rate is the two parts :

$$\frac{da}{dN} = \frac{da}{dN_1} + \frac{da}{dN_2} \tag{18}$$

in which :

N_1 — number of cycles of high frequency stresses

N_2 — number of cycles of high frequency stresses

It follows that the total crack growth rate of the cylinder always exceeds that due to a single set of stresses corresponding rotatory frequency of the crank shaft.

(2) Effect of pressure ratio

Fig. 6 illustrates the variation of maximum stress σ_{max} under constant exhaust pressure and average stress $\bar{\sigma}$ with the pressure ratio, whereas the variations of high frequency stress amplitide $\Delta\sigma_1$ and low frequency stress amplitude $\Delta\sigma_2$ with the pressure ratio are shown in Fig. 7. $\bar{\sigma}$ and σ_{max} drop as $\Delta\sigma_1$ and $\Delta\sigma_2$ increase. Fracture mechanics predict that the crack growth rate is proportional to the average stress strength factor and the amplitude of stress strength factor.

$$\frac{da}{dN} = f(\Delta k, \bar{k}) \tag{19}$$

Thus when pressure ratio rises, Δk increases and $\bar{k}$ decreases, and the variation of $\frac{da}{dN}$ with ε is not merely monotic but follows some functional pattern. It may be surmised that as the pressure ratio increases, there exist for certain ε small or comparatively small values of $\frac{da}{dN}$ which, if maintained, would mean the

life -span of the cylinder obviously, ε_o is influenced by the structure, shape and dimensions of the cylinder. We may, therefore, attempt to optimize the design of the cylinder by varying the shape and dimensions of the cylinder to find the optimal value of pressure ratio with regard to the life-span of the cylinder as predicted by thermo-dynamical analysis.

3. Laboratory Analysis

Fig. 8 shows the plot of radial and tangential strains of the critical points in the inner wall of the cylinder as measured by the specially installed device. The manner of variation so illustrated basically agree with analytical results, and it reasserts the previous conclusion that, under pulsative pressures, the pulsation of strain (stress) is the superposition of the pulsations due to stresses of low frequency and large amplitude and stresses of high frequency and small amplitudes.

V CONCLUSION

1. Results from FEM analysis and actual tests both indicate that high stress peak values exist on the outer boundary of the xoy plane of the cylindr's exhaust opening, and higher peak values are also likely to exist at similar locations on the inner boundary of cylinder cover.

2. The stresses in a high pressure cylinder are compsised of low-frequency, large-amplitude stresses and high-frequency small-amplitude stresses. As the pressure ratio increases, the amplitudes of both low and high stresses increase accordingly.

3. For every particular high pressure cylinder, an optimal value for pressure ratio with regard to strength may be obtained, and, by varying the structural dimensions, the optimal result of good pressure ratio with regard to strength and satisfying thermo-dynamical calculations can be achieved.

REFERENCES

[1] Wang Di-sheng : The working stress and an analysis on the fracture of the integral type of high pressure cylinders.

[2] Wang Di-sheng , et el : An Finite Element Analysis

of High Pressure Cylinder Compressor Technology.

[3]. Wang Di-sheng : A criterion for the reliability of the compressor's high pressure cylinder. (Journal of the Xi'an Jiao Tong University)

[4]. Deuous, C. Gazis · Exact Analysis of the Pane-strain Vibration of Thick-walled Hollow Cylinder. Vol.30, No.8, ASME 1958.

[5]. B.D. Goldthorps · Crack Growth in Pressurized Thick - walled Cylinder.

[6]. W.R. Buell & B.A. Bush · Mesh Generation --- A Survey · Journal of Engineering for Industry. Trans. of the ASME, Series B. Vol. 95 · No.1. Feb.1973. pp. 332-338.

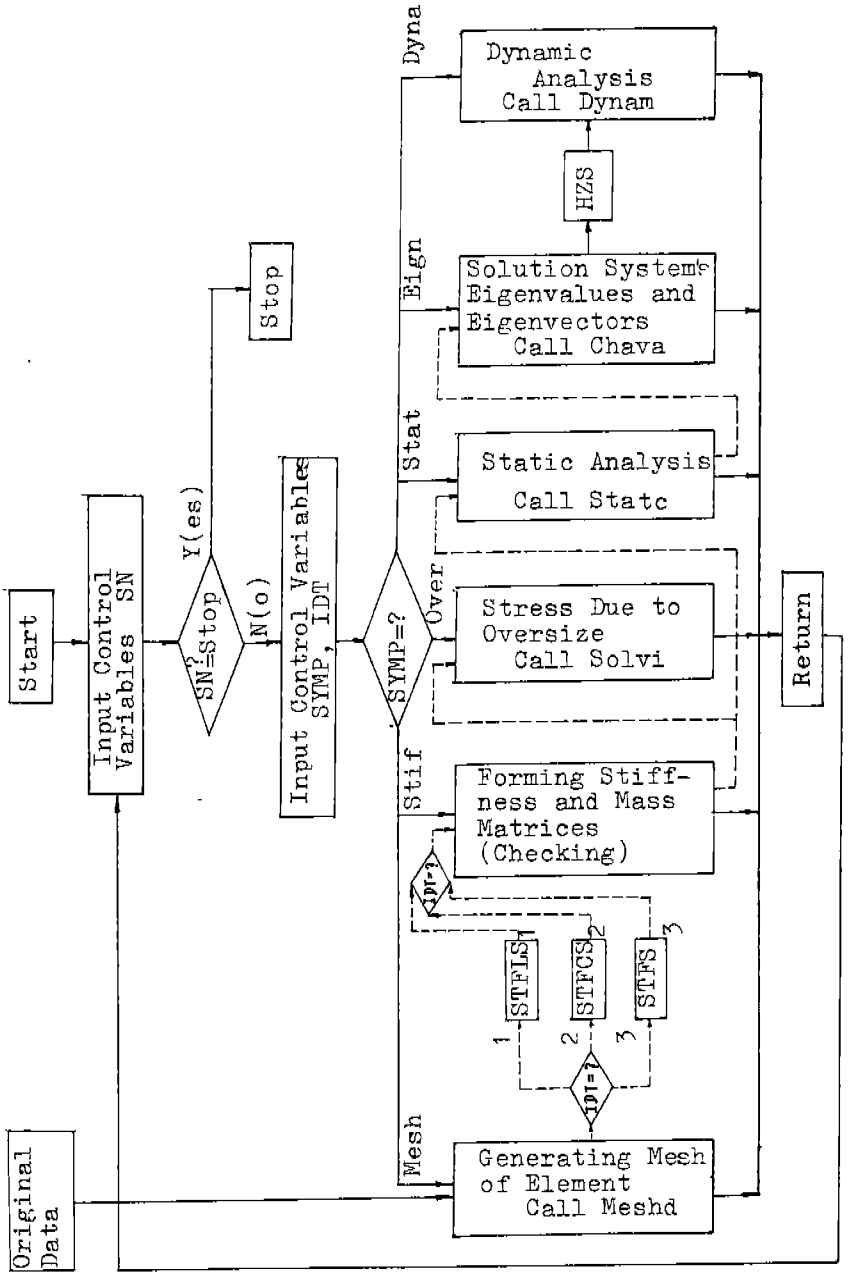

Fig. 1 Flow-chart for Computation of High Pressure Cylinder Stresses

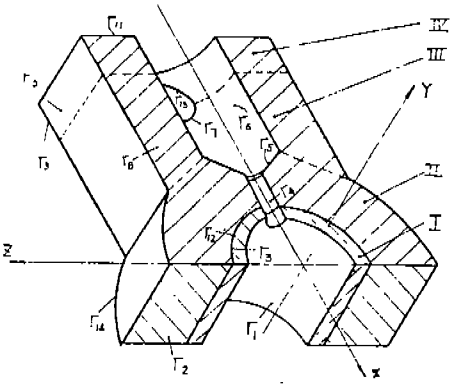

Fig. 2 Schematic representation of intersection between valve and cylinder chamber (only shown $\frac{1}{4}$)

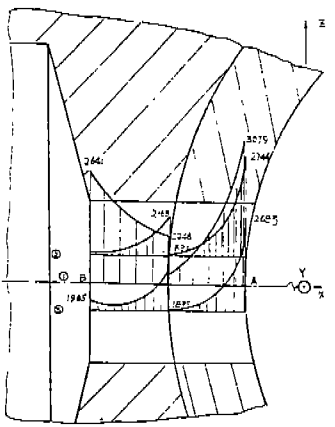

Fig. 3 The stress distribution along the $\bar{z}$ direction of plate bore.

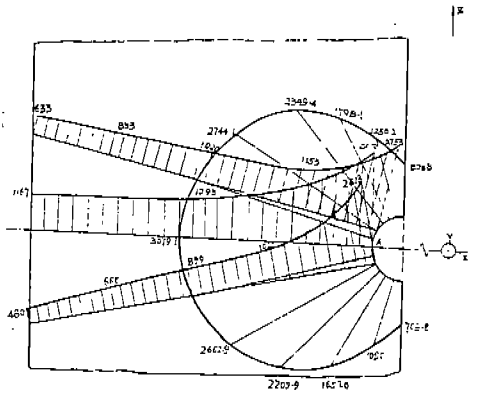

Fig. 4 The stress distribution along the radial direction of the plate bore.

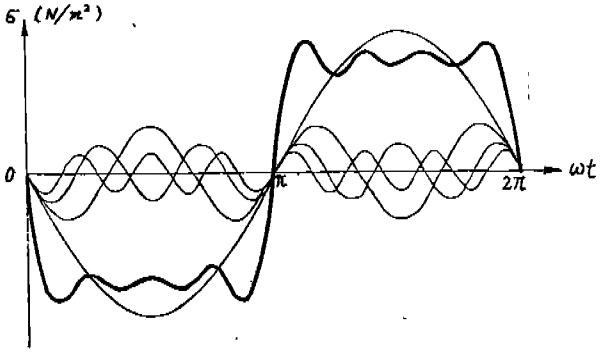

Fig.5 Stress variation due to the gaseous forces of first 4 modes.

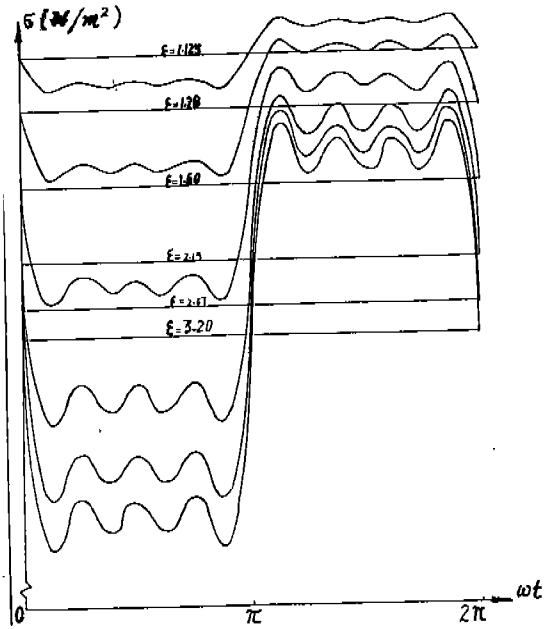

Fig. 6(a) Effect of pressure ratio on average stress and maximum stress.

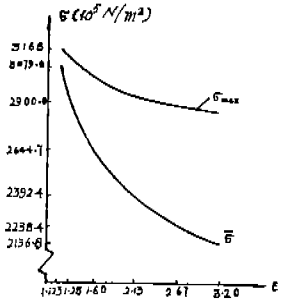

Fig. 6(b) The variation of maximum stress and average stress with the pressure ratio

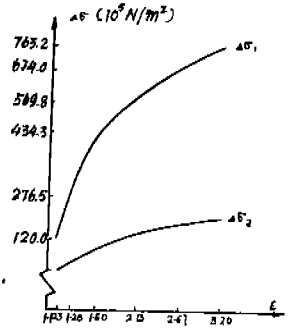

Fig. 7 Effect of pressure ratio on stress amplitude

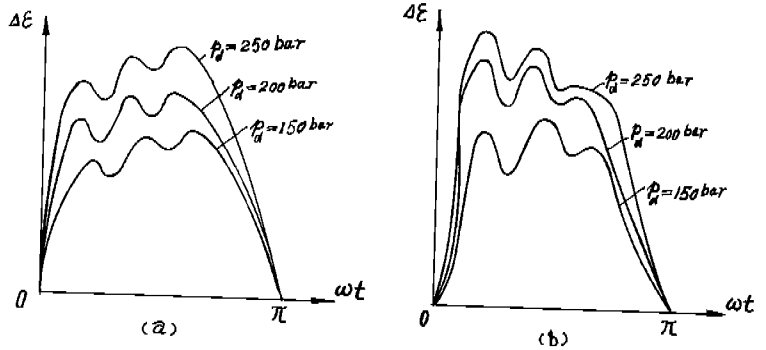

Fig. 8 The plot of radial(a) and tangential(b)strains of the critical points in the inner wall of the cylinder.